Journal of Materials Chemistry C

ROYAL SOCIETY OF CHEMISTRY

PERSPECTIVE

View Article Online
View Journal | View Issue

Cite this: J. Mater. Chem. C, 2022, 10, 4546

Application of time-resolved electron paramagnetic resonance spectroscopy in the mechanistic study of thermally activated delayed fluorescence (TADF) materials

Xi Chen, Xiao Xiao and Jianzhang Zhao *

Received 13th October 2021,
Accepted 13th December 2021

DOI: 10.1039/d1tc04888k

rsc.li/materials-c

Triplet exciton harvesting is crucial in organic light emitting diodes (OLEDs) because the triplet states produced by electron and hole recombination account for up to 75% of the total excitons, whereas the singlet states account for 25%. However, the triplet state of organic molecules is usually either non-emissive at room temperature or gives very long phosphorescence lifetimes, both of which are detrimental to OLEDs. Thermally activated delayed fluorescence (TADF) emitters are one answer to this challenge. Typical TADF emitters are based on an electron donor–acceptor structure motif, and the low-lying states include the charge transfer singlet (^{1}CT) state and triplet (^{3}CT) state, and a closely-lying localized triplet (^{3}LE) state. Although many efficient TADF emitters have been developed for OLEDs, the underpinning photophysical processes of TADF, for instance, the charge separation, the forward intersystem crossing (ISC) and the reverse ISC (rISC), and the coupling of the excited states of these emitters, are far from clear. Herein, we introduce recent developments in the study of the photophysical processes of TADF emitters using the time-resolved electron paramagnetic resonance (TREPR) spectroscopy method. This spectral tool supplies unique information on the dynamics of the transient paramagnetic species involved in the TADF processes, for instance, the ^{3}CT and the ^{3}LE states, as well as the ISC mechanisms. Physical insights have been obtained with TREPR spectra on the TADF mechanism, such as simultaneous observation of the ^{3}CT and ^{3}LE states, vibrational and spin-vibronic coupling mediated ISC, and the electronic configuration and spatial delocalization of the ^{3}CT and ^{3}LE states' wave functions. Factors beneficial to TADF obtained *via* theoretical computations are also briefly introduced.

1. Introduction

Organic light emitting diodes (OLEDs) have attracted much attention in recent years.[1–7] One of the critical issues in the research of OLEDs is to develop efficient emitters to harvest both the singlet and the triplet excitons for efficient light emission. According to the electron spin statistics, the singlet and triplet states are formed at the rates of 25% and 75%, respectively, from the electron–hole recombination in the emitting layer of the OLED devices. For organic fluorescence emitters, the maximal internal quantum efficiency is 25% (IQE, without any other processes considered, such as triplet–triplet-annihilation, TTA). Therefore, phosphorescence emitters were developed as second generation emitters for OLEDs, for which the maximal IQE is 100%, because both the singlet and triplet excitons can be harvested for light emitting. In ordinary phosphorescent transition metal complexes, the ultrafast inter-system crossing (ISC) transforms the singlet state to the emissive (phosphorescent) triplet excited state.[5,8–11] However, the phosphorescent transition metal complexes, for instance those contain Pt(II) or Ir(III) atoms,[12–14] suffer from high cost, toxicity, *etc.* Therefore, it is desired to develop new emitting materials for OLEDs to address the above challenges, for instance, neat organic emitting materials without any precious metal atoms. This is a challenge in molecular photochemistry, because organic molecules usually do not exhibit phosphorescence at room temperature or they exhibit long phosphorescence long lifetimes.[15]

Recently, Adachi *et al.* proposed to use organic compounds showing thermally activated delayed fluorescence (TADF) as light emitting materials for OLEDs.[16,17] Different from the normal organic fluorescence emitters, both the singlet and the triplet excitons can be harvested in TADF emitters for light emission. In other words, for TADF molecules, both the singlet and the triplet states of the emitters are formed in the OLED devices; although the triplet excitons are usually non-emissive, it can be transformed to the emissive singlet states *via* reverse

State Key Laboratory of Fine Chemicals, School of Chemical Engineering, Dalian University of Technology, E-208 West Campus, 2 Ling Gong Road, Dalian 116024, P. R. China. E-mail: zhaojzh@dlut.edu.cn

ISC (rISC), which is thermally activated. The small energy gap between the singlet and triplet states was believed to make the rISC efficient; thus the non-emissive triplet excited state is harvested for light emission and the luminescence lifetime is short (in the range of a few microseconds), which are beneficial for OLEDs. The maximal IQE for the TADF materials is up to 100%. Therefore, these novel materials have attracted much attention in recent years for the development of efficient OLEDs.[3–7,18–25] Moreover, from the photochemistry point of view, TADF materials are also intriguing in the study of fundamental photophysics of charge transfer (CT) and ISC, as well as excited state dynamics.

Upon photoexcitation (note this is different from the scenario in operating OLED devices, in which the TADF materials are electronically excited *i.e.* by electron–hole recombination), charge separation, ISC, rISC, radiative and non-radiative decay of the singlet (normally a charge transfer singlet state, *i.e.* ^{1}CT) and triplet states are involved in the photophysical processes of TADF emitters. It is fundamentally important to unravel these entangled photophysical processes. However, till now no conclusive understanding of this kind of emissive material is achieved. For instance, there is still much room to unravel the excited states involved in the TADF process (is it two states or more), the molecular structural factors (rigid or flexible) that enhance the ISC in these heavy atom-free molecules, and to enhance the overall TADF efficiency.

The photophysical processes of the TADF emitters are complicated. In the early stage of research, only the lowest-lying S_1 and T_1 states were considered, and the studies focused on reducing the energy gap between the S_1 and T_1 states.[17,26–29] However, now there is consensus in the community that an intermediate state should be involved in the TADF process, which is critical for ISC and rISC, such as the localized triplet excited state (^{3}LE).[6,30–32] Generally speaking, upon photoexcitation, either the localized singlet excited (^{1}LE) state or the ^{1}CT state is firstly populated, then ISC occurs, and the ^{3}LE and the charge transfer triplet state (^{3}CT) will be populated. rISC will populate the emissive ^{1}CT state again.[30,31,33,34] It is not a trivial task to discriminate these transient species and to determine their dynamics using time-resolved transient optical spectroscopy; for instance, the optical spectral feature of ^{1}CT and ^{3}CT states should be virtually the same. Note the electron exchange energy in this case is very small; considering the negligible spatial overlap of the molecular orbitals, the spin–spin interaction of the radical anion and cation is also much weaker as compared to the LE states; as a result, the energy gap between the two states is small, and the difference between the ^{1}CT and ^{3}CT states is mainly the electron spin angular momentum, not the electronic configuration.[35–37] In other words, the UV-vis absorption of the ^{1}CT and ^{3}CT states will be virtually the same. Moreover, the mechanism of the formation of the ^{3}CT state is unclear; it should either be direct $^1\text{CT} \rightarrow {}^3\text{CT}$ or an intermediate ^{3}LE state should be involved. The ^{3}LE state of the TADF molecules may be different from the triplet state of the components of the molecule (electron donor and acceptor), because the TADF molecules are usually compact electron donor–acceptor polyads, *i.e.* the electron donor and acceptor are connected with a short linker, and delocalization of the wave function of the triplet state may occur.[31] Direct spin orbit coupling (SOC), vibrational coupling or spin-vibronic coupling may all enhance the ISC of the TADF emitters. Transient optical spectroscopy can hardly provide direct experimental evidence to discriminate these species or the photophysical processes.

In this perspective article, we summarized the recent development in the mechanism studies on the TADF materials, we focus on the study of small organic molecules based on an electron donor–acceptor motif, by using time-resolved electron spin paramagnetic resonance (TREPR) spectroscopy. TREPR spectra may provide information on the transient paramagnetic species involved in the TADF process, such as the ^{3}CT state, or the radical pair, and the precursor of the ^{3}LE states, the spatial localization of the triplet state wave function, and the ISC mechanisms.[37–44] Some methods based on magnetic field effect have been developed for studying organic semiconductors including magneto-electroluminescence (MEL), optically detected magnetic resonance (ODMR) and magneto-conductance (MC). However, these methods are mainly based on the change in the electroluminescence intensity or electrical conductance of the device with the magnetic field changes. They are not appropriate for organic compounds showing TADF; among the other aspects, the ^{3}CT and ^{3}LE states of the TADF materials are non-emissive. On the other hand, TREPR spectroscopy is a technique for the characterization of the paramagnetic transient species of TADF materials upon photoexcitation. For instance, the electron spin selectivity of ISC, the zero field splitting (ZFS) D and E parameters (the electron spin distribution) of the triplet state, and the origin of the paramagnetic species can be well characterized with the TREPR spectra. Moreover, it is difficult, if not impossible, to discriminate ^{1}CT and ^{3}CT states by the transient optical spectroscopic methods, such as the femtosecond (fs) or nanosecond (ns) transient absorption (TA) spectroscopy, due to the weak spin–spin interaction of the radical anion and cations, as the electronic transition is literally the same for ^{1}CT and ^{3}CT states. Moreover, the delocalization feature of the ^{3}CT and ^{3}LE states in the TADF process can be characterized by TREPR spectra, but not the transient optical spectral methods.

For TREPR spectroscopy, the paramagnetic transient species are selectively detected, such as the spin polarized radicals formed in the reactions, or the spin polarized triplet excited states. The ^{3}CT state will give a TREPR signal, whereas the ^{1}CT is TREPR spectral silent. The magnitude of the spin–spin interaction of the radical anion and cation of the ion pairs, and the spatial confinement of the triplet state wave function, can be directly quantified with the ZFS parameters (D and E values) of the triplet states. The sign of D depends on the shape of the spin density distribution of the triplet state. D is positive ($D > 0$) when the spin density distribution is in the oblate shape and D is negative ($D < 0$) when the electron spin distribution is in the prolate shape. Hyperfine coupling parameter determined using the Electron–Nuclear DOuble Resonance (ENDOR) technique allows precise determination of the extent of delocalization of the triplet state.[45,46] Moreover, the electron spin dynamics can be studied with the TREPR

spectra, for instance, the precursor of the ^{3}LE state can be identified or in other words, the ISC mechanism involved in the TADF emitters can be discriminated by the TREPR spectra.[47,48] The ordinary SOC enhanced ISC, the hyperfine interaction (HFI) enhanced ISC, vibrational enhanced ISC or the ISC facilitated by the spin-vibronic coupling may be all involved in TADF. These different ISC mechanisms can be readily discriminated by the specific electron spin polarization (ESP) phase pattern of the triplet TREPR spectra of the TADF molecules upon photoexcitation (in some cases the analysis should be aided by theoretical computation).[40] TREPR spectroscopy has been intensively used in study of the transient, spin-polarized free radicals and the spin correlated radical pairs (SCRP), the ^{3}CT states and the ^{3}LE states.[36,39–41,49,50] Recently, TREPR spectroscopy has also been used in study of TADF molecules; unique insights on the photophysical processes have been obtained. Recent development in the application of TREPR spectra in study of the photophysical processes of TADF emitters is summarized in this article.

2. TREPR spectroscopy: detection of the transient paramagnetic species and the ISC mechanisms involved in TADF

2.1 Observation of localized triplet states: different ISC mechanisms

In 2015, Ikoma *et al.* studied a few representative TADF emitters using TREPR spectroscopy (Fig. 1).[51] The molecular structures of the compounds are with carbazole or phenoxazine as the electron donor, and cyanobenzene or triazine as the electron acceptor. Note the π-conjugation planes of the donor and acceptor units adopt orthogonal geometry as a result of the conformation restriction of the bulky moieties and the congested microenvironments of the moieties.[51] Experiments show that the external quantum efficiencies (EQEs) of these TADF emitters in OLED devices are 19.3%, 12.5%, 6.0% and 5.3% for **4Cz-IPN**, **PXZ-TRZ**, **Cz-T** and **PIC-TRZ**, respectively.

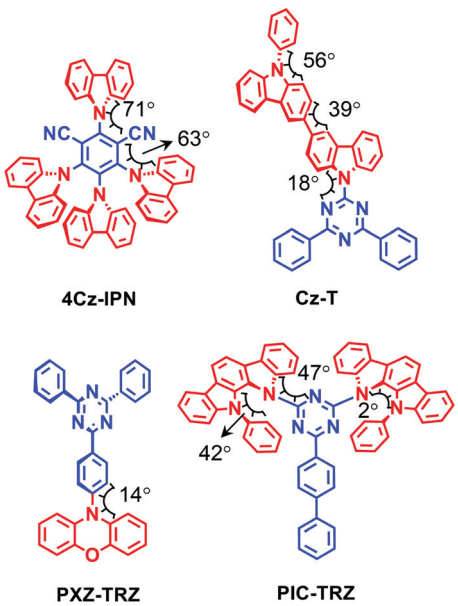

Fig. 1 Molecular structures of the typical TADF emitters.

The TREPR spectra of the randomly oriented molecules of these TADF emitters in frozen solution (solvent: toluene) at 77 K were recorded (Fig. 2). For the compounds showing high EQE, *i.e.* **4Cz-IPN** and **PXZ-TRZ**, the ESP at the six canonical orientation are (*a*, *e*, *e*, *a*, *a*, *e*) and (*a*, *a*, *e*, *a*, *e*, *e*), respectively. For the compounds showing lower EQE, *i.e.* **Cz-T** and **PIC-TRZ**, the ESP of (*e*, *e*, *e*, *a*, *a*, *a*) was observed for the triplet TREPR spectra. Moreover, the TREPR spectra of **Cz-T** and **PIC-TRZ** have a larger width than the those of **4Cz-IPN** and **PXZ-TRZ**. For **Cz-T** and **PIC-TRZ**, a single component based on the normal SOC-induced ISC is sufficient to simulate the experimental spectra. For the compounds showing a high EQE, triplet states formed by two ISC mechanisms, *i.e.* the SOC ISC and the HFI enhanced ISC, are required to attain a satisfactory simulation. These two different ISC mechanisms are illustrated in Fig. 3. Moreover, simulation shows that the ZFS *D* parameters of **4Cz-IPN** and **PXZ-TRZ** (46 mT and 49 mT) are much smaller than the triplet state of the native cyanobenzene ($|D|$ = 147 mT) or the triplet state of triphenyl-*s*-triazine ($|D|$ = 133 mT). The decreased ZFS *D* parameter is an indication that the transient species is with significant delocalization or CT character, although the authors proposed that the transient species is the delocalized triplet state (the argument is the non-vanishing ZFS *E* parameter). The population ratios of the triplet state formed by HFI and the SOC ISC mechanisms, respectively, are 0.50 and 0.36 for **4Cz-IPN** and **PXZ-TRZ**, respectively. Recently Brédas and Adachi *et al.* studied **4Cz-IPN** using experimental and theoretical methods, and they proposed that an upper triplet state localized on partial molecular structure is involved in the TADF process (supported by transient absorption spectral study, and the uphill feature of ISC), and the energy of these states localized on partial molecular structure is lower than that of the

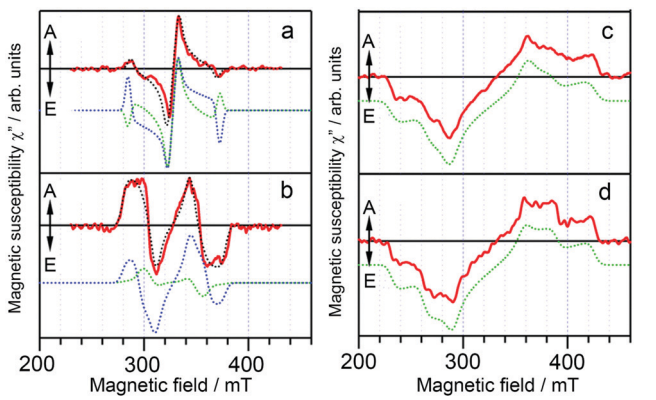

Fig. 2 Transient EPR spectra for (a) **4Cz-IPN**, (b) **PXZ-TRZ**, (c) **Cz-T**, and (d) **PIC-TRZ** in toluene detected at 550 ns after a laser flash at 77 K (red solid lines). The dotted lines are the simulation spectra: green, SOC-induced polarization; blue, hyperfine coupling (HFC)-induced polarization; and black, SOC plus HFC-induced polarization. Reproduced with permission.[51] Copyright 2015, American Chemical Society.

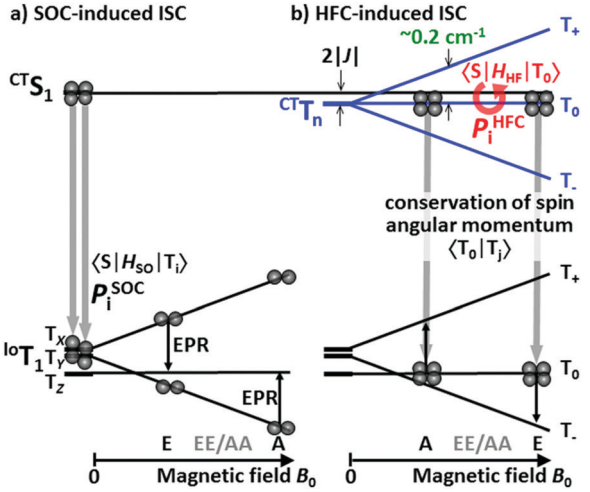

Fig. 3 Spin polarization mechanisms for the T_1 state due to ISC from the S_1 state under an external magnetic field along the *z* axis of the molecule. (a) The SOC-induced ISC. (b) HFC-induced ISC. Reproduced with permission.[51] Copyright 2015, American Chemical Society.

carbazole triplet state (*ca.* 3.08 eV).[34] They also found that the low-lying triplet state of **4Cz-IPN** has a significant CT character, the triplet state is neither localized on the carbazole nor the cyanobenzene moieties, but delocalized on the carbazole and cyanobenzene parts.[34] A TREPR spectral study on the reference compounds (partial structure of **4Cz-IPN**) will be useful to fully unravel the photophysical process.

For **Cz-T** and **PIC-TRZ**, a SOC ISC induced triplet state was observed, with the T_X and T_Y sublevels overpopulated. The ZFS *D* parameter of the triplet state of these compounds is 97 mT, very close to the triplet state of triphenyl-*s*-trazine ($|D|$ = 133 mT). Thus it was proposed that the triplet state of **Cz-T** and **PIC-TRZ** is spatially confined. Due to the clear trend correlation between the EQE value and the triplet state TREPR features, the authors proposed that efficient TADF molecules should undergo radical pair ISC (RP-ISC).[51] The difference between the SOC-induced ISC and the HFI induced ISC is illustrated in Fig. 3. For the SOC ISC mechanism, the in plane T_X and T_Y sublevels are mainly populated, then the transfer of population rates to the T_+ and T_- sublevels under external magnetic fields occurs, and the (*e*, *e*, *e*, *a*, *a*, *a*) ESP phase pattern is observed for the triplet state. For the HFI induced ISC mechanism (*i.e.* the RP-ISC mechanism), mainly the T_0 sublevel is populated, because of the smaller energy gap between this sublevel and the S_1 state (in CT feature, Fig. 3). Under this circumstance, a special (*a*, *e*, *e*, *a*, *a*, *e*) or (*e*, *a*, *a*, *e*, *e*, *a*) ESP phase pattern will be observed for the triplet state. This kind of unique ESP phase pattern is inaccessible for the triplet state formed *via* the normal SOC ISC mechanism.

Considering the high T_1 state energy of the carbazole unit (*ca.* 3.06 eV),[52] and the CT state energy (*ca.* 2.69 eV, approximated by the crossing point of the normalized UV-vis absorption and the CT emission spectra),[51] it is likely that the CT state, or ^{3}LE state with significant delocalization, should be observed in the TREPR spectra. This is supported by the unusually small ZFS *D* parameter observed for **4Cz-IPN** and **PXZ-TRZ**. More evidence was presented by femtosecond and nanosecond transient absorption (fs-TA and ns-TA),[53] which show that a delocalized CT state and ^{3}LE state were observed for **4Cz-IPN** (the charge resonance effect), *i.e.* the positive charge is delocalized in the carbazole moieties, indicated by the near IR absorption band in the transient optical absorption spectra. However, it should be noted that the TREPR spectra of the triplet state is usually measured in a frozen solution at cryogenic temperature (*e.g.* 80 K or even lower), to suppress the tumbling of the molecules and spin lattice relaxation (SLR); the solvation effect in this case is missing, which makes the CT energy higher than that in fluid solution at room temperature.

The molecular structure features of the compounds presented in Fig. 1 deserve more analysis. For **4Cz-IPN**, the carbazole moieties are in a sterically congested microenvironment; this will make the donor and the acceptor take an orthogonal (perpendicular) geometry. A study on analogue molecules shows that the highest occupied molecular orbital (HOMO) and lowest unoccupied molecular orbital (LUMO) are spatially separated.[17,20,54] In this case, the ^{1}CT $\rightarrow$ ^{3}LE may be enhanced by spin orbit charge transfer ISC (SOCT-ISC).[37,55–58] With the purpose of design of heavy atom-free triplet photosensitizers based on the electron donor–acceptor molecular structure, the orthogonal geometry is beneficial for the SOCT-ISC.[37,56,57,59] This is also applicable to TADF emitters.[31] Moreover, the electron exchange integral for the electrons in the frontier molecular orbitals (MOs) of the CT state is small, which results in an extremely small ^{1}CT/^{3}CT energy gap. This small energy gap is beneficial for the HFI induced ISC (RP-ISC); however, the slow kinetics of HFI concerning ISC, and the weak coupling of the two states (^{1}CT and ^{3}CT) with same electronic configuration but different spin multiplicity (which is against El Sayed's rule for ISC), makes ^{1}CT $\rightarrow$ ^{3}CT an unlikely channel to populate the triplet state significantly,[31,48] *i.e.* the population of the ^{3}CT state is probably mediated by the ^{3}LE state. For **PXZ-TRZ**, the phenothiazine and the triazine units are separated by an intervening phenyl linker, which is also beneficial for attaining small *J* values. For **Cz-T** and **PIC-TRZ**, the steric hindrance is not significant; the molecules may adopt a more planar geometry, which is detrimental to the RP-ISC and the SOCT-ISC.

In the early stage of the study of TADF emitters based on the electron donor–acceptor molecular structure motif, the research was focused on reducing the energy gap between the lowest-lying S_1 and T_1 states, and increasing the molecular rigidity; it was believed both are beneficial to TADF. However, recent experimental and theoretical studies show that this is not true, and an intermediated dark state, *i.e.* ^{3}LE state, should be involved in the TADF process.[30,31,33,60] For instance, it was found that electron donor–acceptor TADF emitters with similar S_1/T_1 state energy gaps may show significant variation in the rISC rate constants, and the rigid molecular structure (or hindered rotation) leads to suppression of rISC and thus TADF, causing the phosphorescence to turn on.[61] With vibronic coupling between the ^{3}CT and ^{3}LE states considered, much faster ISC and population of ^{3}LE states were observed. On the other hand, the HFI effect on the ISC rate constants is

negligible (in the ns range).[30] Calculations also show that the smaller energy gap between the S_1 and T_1 states is beneficial for ISC to produce the ^{3}LE state. Computation on the rISC process shows that the vibronic coupling between the ^{3}LE and ^{3}CT states plays a significant role in the rISC kinetics. These results indicates that not only the energy gap of the S_1/T_1 states is important, but also the energy gap and the spin-vibronic coupling between the ^{3}CT and ^{3}LE states. For the latter case, restricting the molecular conformation does not necessarily enhance TADF as previously thought, it may inhibit rISC thus reducing the TADF performance.[30]

Monkman *et al.* confirmed that the energy gap between the ^{3}LE state and the CT state of the donor–acceptor–donor triad imposes a significant effect on the rISC kinetics and thus the TADF performance, using photo-induced absorption spectra with varying host rigidities and polarities (the CT state energy level or the intramolecular motion).[33] This model states that the coupling between the ^{1}CT and ^{3}CT states is mediated by non-adiabatic coupling (the non-Born–Oppenheimer effect; second order perturbation) between the ^{3}LE and ^{3}CT states, which is spin-vibronic coupling for the latter; both the ^{1}CT → ^{3}CT ISC and the rISC of ^{3}CT → ^{1}CT are greatly enhanced. However, it should be noted that these principles are probably not applicable for compounds showing TADF, but have a single chromophore molecular structure profile, *i.e.* not based on the electron donor–acceptor structure profile.[16,62]

In 2018, Greenham *et al.* reported experimental evidence for vibrationally assisted ISC in TADF emitters with TREPR spectra.[63] They studied the TREPR spectra of two benchmark TADF emitters **4Cz-IPN** and **2Cz-PN** (Fig. 4), and made a different interpretation of the TREPR spectra and the photophysics of **4Cz-IPN**. The key finding is that the SOC-mediated ISC is triggered by thermally populated torsion vibrational modes of the emitters, *i.e.* the vibronic coupling plays a significant role in TADF, and no HFI effect is involved in the ISC of the TADF emitters of **2Cz-PN** and **4Cz-IPN** (Fig. 5). The authors found that the SOC matrix elements' (SOCMEs) magnitudes of the ISC from S_1 to the T_X, T_Y and T_Z sublevels of the T_1 state do not match with the experimentally observed population rates of the three sublevels. Thus factors other than the pure electronic model play a role in enhancing the ISC. Moreover, satisfactory simulation of the TREPR spectra of both **2Cz-PN** and **4Cz-IPN** can be achieved without invoking the HFI effect, while vibronic coupling plays a signal role in ISC. If only the direct SOC is considered, according to the calculated SOC matrix element magnitude, the population of $T_{1,a}$ and $T_{1,b}$ should be negligible, and the population of $T_{1,c}$ should be close to 1. However, this prediction does not agree with the experimental observations that show the three sublevels are almost homogenously populated. Instead, considering the geometry fluctuation, caused by the rotation freedom of the carbazole moieties driven by thermal energy at 300 K, the SOCMEs are increased, and ISC is enhanced. Computations

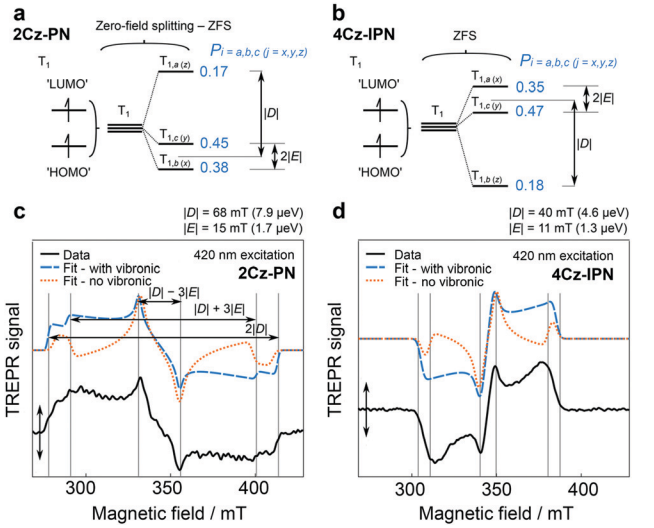

Fig. 5 ZFS diagram for (a) prolate **2Cz-PN** and (b) oblate **4Cz-IPN**, indicating fitted $|D|$ and $|E|$ parameters. TREPR spectra (80 K) for toluene solutions of (c) **2Cz-PN** (420 nm excitation) and (d) **4Cz-IPN** (460 nm excitation), shown as black solid lines. Spectra were recorded 0.4 μs after laser excitation (0.04 μs averaged). Vertical lines overlaid on the spectra denote canonical orientations of ZFS principal axes with respect to the magnetic field, and can be used to derive $|D|$ and $|E|$ as shown in part c. Fits "with vibronic" and for "no vibronic" contributions to ISC are presented as blue dashed lines and yellow dotted lines, respectively. Reproduced with permission.[63] Copyright 2018, American Chemical Society.

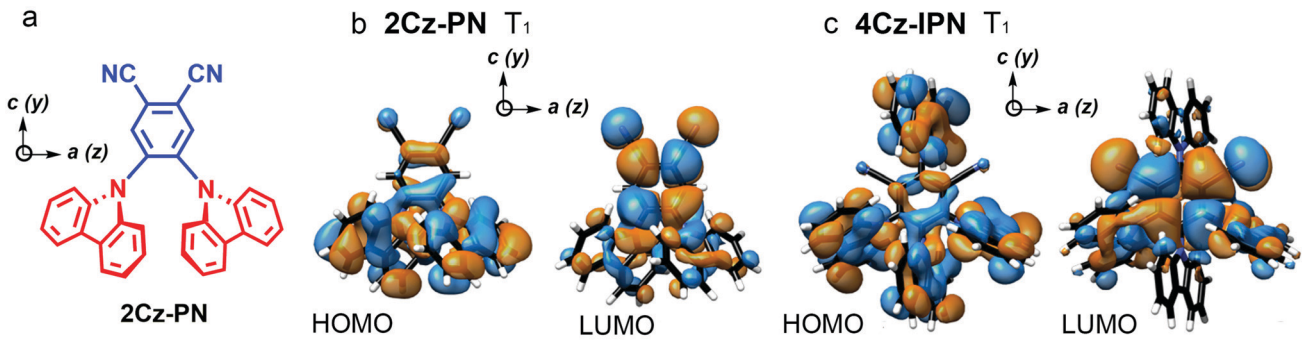

Fig. 4 (a) Molecular structures of **2Cz-PN**. UKS-DFT-calculated canonical orbitals for the T_1 states of (b) **2Cz-PN** and (c) **4Cz-IPN**, using the PBE0 functional and EPR-II basis set. *a*, *b*, and *c* and *x*, *y*, and *z* denote the symmetry and ZFS axes, respectively. Reproduced with permission.[63] Copyright 2018, American Chemical Society.

also show that the dynamic SOCMEs of **4Cz-IPN** are almost homogeneous for ISC to the three sublevels of the T_1 state; experimentally the population rates of the three sublevels are P_a = 0.35, P_b = 0.18, and P_c = 0.47, respectively. Similar results were observed for **2Cz-PN**.[63] Thus, the authors proposed that ISC is enhanced by vibration; mainly the rotation about the linker. Thus, increasing the molecular rigidity of TADF emitters may be counterproductive to their emission properties. It should be pointed out that in this model, only two states were considered (S_1 and T_1).

2.2 Simultaneous observation of ^{3}LE and ^{3}CT states with TREPR spectra

TADF properties are not restricted to any specific molecular structural motif.[3–6,59,64] Any compounds with closely-lying ^{1}CT, ^{3}CT and ^{3}LE states may exhibit TADF properties (or more generally, close-lying S_1/T_1 states).[65,66] Recently, we prepared a compact, orthogonal electron donor–acceptor dyad, with naphthalimide (NI) as the electron acceptor and phenothiazine (PTZ) as the electron donor (Fig. 6).[67] The connection (linker or bridge) between the NI and the PTZ moieties is different in the two dyads. In **NI-N-PTZ**, the connection is at the N-position of the PTZ moiety, thus due to steric hindrance from the H atom at the 5-position of the NI moiety (*peri*-position), the π-planes of the two moieties take orthogonal geometry, and the electronic coupling of the donor and acceptor is small. For **NI-C-PTZ**, however, the connection is at the 3-position of the PTZ moiety; smaller steric hindrance is expected, resulting in stronger electronic coupling between the donor and the acceptor. This postulate is confirmed by the observation of a weak CT absorption band (ε = 580 M^{-1} cm^{-1} at 450 nm) for **NI-N-PTZ**, while a much stronger CT absorption band was observed for **NI-C-PTZ** (ε = 9000 M^{-1} cm^{-1} at 405 nm).[67] Moreover, a larger ^{1}CT/^{3}CT energy gap is anticipated for **NI-C-PTZ**, due to the strong electronic coupling between the donor and acceptor in this dyad. CT emission bands were observed for both dyads; the ^{1}CT state energies of the two dyads are approximated as 2.25 eV and 2.75 eV, respectively, by the on-set of the CT emission band

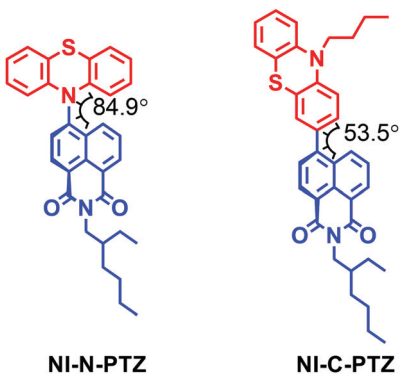

Fig. 6 Molecular structure of **NI-N-PTZ**, which shows TADF properties. The molecular structure of the reference compound **NI-C-PTZ** is also presented. Reproduced with permission.[67] Copyright 2019, American Chemical Society.

(in hexane).[67] The ISC and the rISC in **NI-N-PTZ** may be enhanced by the orthogonal orientation of the PTZ and the NI moieties, *i.e.* the SOCT-ISC mechanism.[37,56–58] Since the T_1 state of the native NI moiety is *ca.* 2.29 eV,[68] we expect TADF only for **NI-N-PTZ**. Indeed TADF was observed only for **NI-N-PTZ** (in hexane at room temperature), and the luminescence decay trace shows a distinct biexponential feature, 22.6 ns (96.6%)/ 2.6 μs (3.4%). Normal prompt fluorescence was observed for **NI-C-PTZ**, with a fluorescence lifetime of 3.4 ns. This is one solid evidence that given the CT state energy is much higher than the ^{3}LE state, no TADF will be resulted, even if ^{1}CT and ^{3}CT states are separated by a small energy gap. A ns-TA spectral study shows that a CT state was observed for **NI-N-PTZ** (Fig. 7a; in hexane).[67] The strong positive absorption band in the ns-TA spectrum centered at 420 nm is assigned to the NI radical anion ($NI^{-\bullet}$), whereas the PTZ radical cation ($PTZ^{+\bullet}$) shows an absorption band centered at 519 nm. The lifetime of the CT state was determined as 2.6 μs, which is in good agreement with the delayed luminescence lifetimes of the dyad. It is significant to observe such a long-lived CT state in a compact electron donor–acceptor dyad. This result indicates that the CT state is lower in energy than the ^{3}NI state, otherwise the ^{3}NI state should be observed in the ns-TA spectra. However, the energy of the ^{3}NI state should be very close to the CT state for the TADF emitters, and previously it was demonstrated that in some cases, only one of the two triplet states involved in triplet state equilibrium was observed with ns-TA spectra.[69] For **NI-C-PTZ**, however, the ^{3}NI state was observed in the ns-TA spectrum, and the triplet state lifetime was determined as 146 μs.[67]

The triplet TREPR spectrum of **NI-C-PTZ** shows an ESP phase pattern of (*e*, *a*, *e*, *a*, *e*, *a*) (Fig. 7b), which is similar to that observed for 4-bromoNI (**NI-Br**, Table 1).[67] Simulation of the TREPR spectrum of **NI-C-PTZ** gives ZFS *D* and *E* values as 64 mT and 5 mT, respectively (Table 1). Interestingly, the *D* value is smaller than that of the triplet state of **NI-Br** (92 mT), although the *E* parameters are similar for **NI-C-PTZ** (5 mT) and **NI-Br** (5 mT; Table 1). This result indicates that the triplet state of **NI-C-PTZ** is delocalized, and the spin density surface (obtained with theoretical computation) of the T_1 state supports this postulate. For **NI-N-PTZ**, however, satisfactory simulation of the spectrum requires two different triplet states, one is with ZFS $|D|$ and *E* parameters of 49 mT and 9 mT, respectively, which is assigned to the delocalized ^{3}NI state. Another state, however, is with a much smaller $|D|$ value of 32 mT, and the *E* parameter is 0 mT. This is a strong evidence that a ^{3}CT state is observed. This is also in agreement with the ns-TA spectral observation (Fig. 7a). The compact dyad molecular structure of **NI-N-PTZ**, *i.e.* the strong spin–spin interaction between the radical anion and the cation, makes the formation of ^{1}CT and ^{3}CT states possible, otherwise only SCRP can be observed (in this case the electron spin–spin interaction is very weak).[70–72]

Moreover, we observed an evolution of the ESP phase pattern for **NI-N-PTZ**, the ESP is switched at a longer delay time for the ^{3}CT state. This phenomenon is probably due to the interconversion of the ^{3}CT and ^{3}LE states, and rotation of the ZFS principal axes of the ^{3}CT ↔ ^{3}LE internal conversion, and

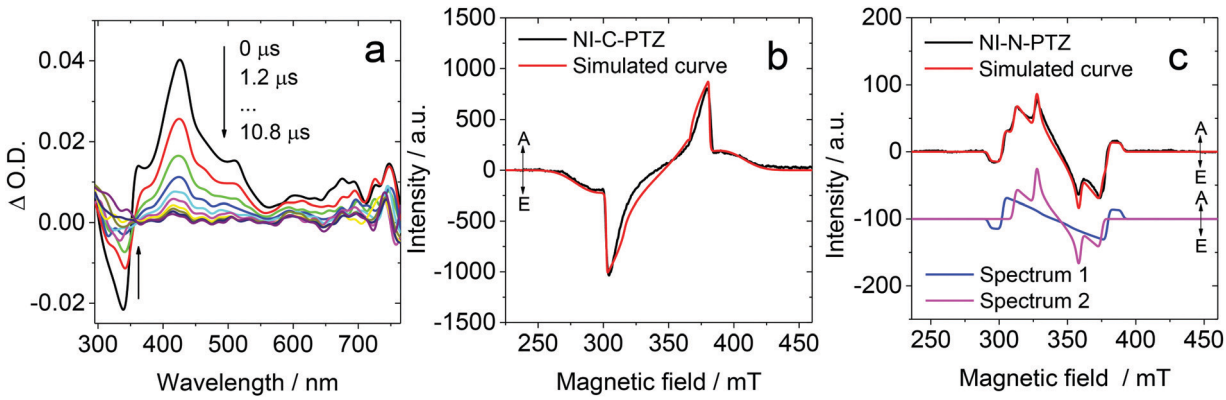

Fig. 7 (a) Nanosecond transient absorption spectra of **NI-N-PTZ** excited at 330 nm. $c = 1.0 \times 10^{-5}$ M in deaerated hexane, 293 K. TREPR spectra of (b) **NI-C-PTZ** and (c) **NI-N-PTZ** determined using a X-band EPR spectrometer, in a frozen solution at 85 K. The delay time is 0.6–0.7 μs following a 355 nm laser pulse, $c = 1.0 \times 10^{-3}$ M in a mixed solvent hexane/toluene (1/2, v/v). The red lines are computer simulations of the triplet state spectra with parameters listed in Table 1 for **NI-Br** and **NI-C-PTZ**. Reproduced with permission.[67] Copyright 2019, American Chemical Society.

Table 1 Zero field splitting parameters ($|D|$ and E) and relative population rates P_x, P_y and P_z of the zero field spin states obtained from simulations of the triplet-state TREPR spectra of the compounds **NI-Br**, **NI-C-PTZ** and **NI-N-PTZ**. Reproduced with permission.[67] Copyright 2019, American Chemical Society

Compound	$\|D\|$ (mT)	E (mT)	P_x	P_y	P_z
NI-Br	92	5	0	0.67	0.33
NI-C-PTZ	64	5	0	0.3	0.7
NI-N-PTZ	32[a]	0[a]	1.0	0	0
	49[b]	9[b]	0[c]	1[c]	0[c]

[a] Component **2** (spectrum 2 in Fig. 7c) of the TREPR spectrum of **NI-N-PTZ**, recorded with a delay time of 0.6–0.7 μs after laser excitation. [b] Component 1 (spectrum 1 in Fig. 7c) of the TREPR spectrum of **NI-N-PTZ**, recorded with a delay time of 0.6–0.7 μs after laser excitation. [c] The population rate due to the SO-ISC or SOCT-ISC mechanism contribution; main contribution from RP-ISC is not shown.

the selective depopulation of the sublevels of the ^{3}CT *via* TADF emission.[73] This phenomenon needs more investigation. For **NI-C-PTZ**, the TREPR signal decays at a longer delay time, without any ESP change. This is an interesting experimental evidence that the ^{3}CT and ^{3}LE states are both involved in the TADF process. Although the ^{1}CT state is silent in TREPR spectral measurement, it is clear that ^{1}CT state is involved in TADF for obvious reason: it is the emissive state in TADF process of the electron donor–acceptor emitters. Determination of the ^{1}CT/^{3}CT states energy gap precisely is not a trivial task. However, since the MOs are separated spatially for ^{1}CT/^{3}CT states, we assume the energy gap between the two is small.[74] Observation of the ^{3}CT and ^{3}LE states simultaneously is a strong evidence that the TADF is not only dependent on the ^{1}CT/^{3}CT state gap, *i.e.* rISC is strongly dependent on another intermediate states.[53] Given that the CT/^{3}LE state energy is large, as for **NI-C-PTZ**, no TADF will be observed. Moreover, these results show that the ^{3}LE state involved in the TADF process may have a significant CT character, or delocalization.[63]

Besides the TADF approach, another method is to use the TTA to break the limitation of the 25% IQE for the fluorescence emitters in OLEDs. Recently, the exploitation of hot exciton was proposed, *i.e.* the use of $T_n \rightarrow S_1$ ISC in OLED devices to increase the quantum efficiency.[7] This mechanism usually involves the lowest singlet excited state S_1 and a close-to-resonant triplet excited state (T_n), both of which display a hybrid charge transfer-locally excited (HLCT) character to ensure the best compromise between high singlet radiative decay rates, small energy separation and fast triplet-to-singlet conversion.[7] However, the T_n state is difficult to be detected due to its short lifetime.

Oliver, Samuel and Zysman–Colman studied two dyads showing TADF based on the approach of exploitation of hot exciton (Fig. 8).[75] Both compounds show luminescence decay traces with biexponential feature, for instance, **DPA-AnCN** shows a luminescence lifetime of 26.3 ns (98%)/858 ns (2%) in hexane. Since the T_1 state (1.76 eV) is significantly lower than the T_2 state (2.52 eV) and the emissive S_1 state (2.50 eV), it is obvious that the normal TADF is not responsible for the delayed fluorescence of the compound.

The TREPR spectra of the two compounds in a frozen solution in acetonitrile at 80 K were recorded (Fig. 9). For **DPA-AnCN**, two triplet states were required for satisfactory simulation of the experimental TREPR spectra, the first triplet state has a ZFS D value of 61 mT, and the second triplet state shows a narrower TREPR spectrum; a ZFS D parameter of 25 mT was obtained by simulation. The first one is attributed to the T_1 state localized on the anthryl moiety, *i.e.* it is the ^{3}LE state. Note the ZFD D parameter is very close to the value of the triplet

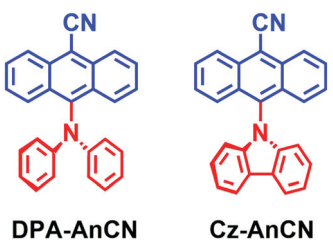

Fig. 8 Anthracene based donor–acceptor derivatives showing delayed fluorescence based on exploitation of hot exciton.

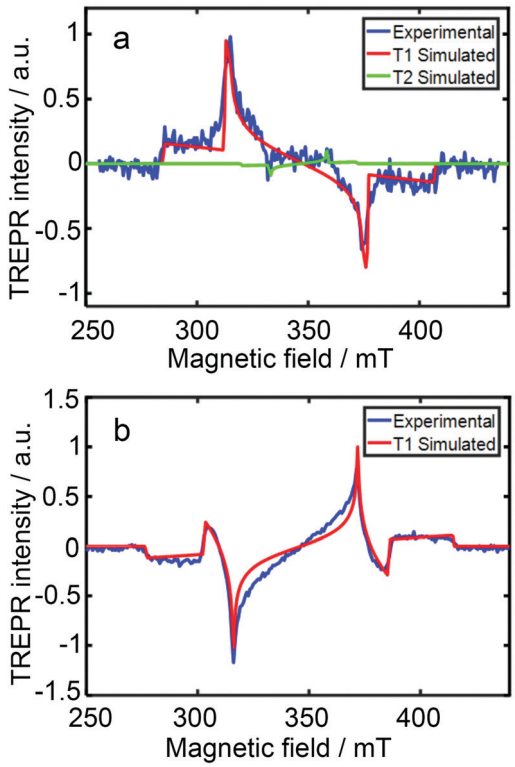

Fig. 9 TREPR spectra at 80 K (blue line) of (a) **DPA-AnCN** and (b) **Cz-AnCN** in toluene solution (10 mg mL^{-1}) recorded 1.5 μs after 532 nm and 410 nm laser pulses, respectively. The best-fit spectral simulations of T_1 (red line) and T_2 (green line) are presented. Reproduced with permission.[75] Copyright 2020, Royal Society of Chemistry.

state of the native anthracene (*ca.* 77–78 mT).[48,76] The second narrower spectrum is attributed to the T_2 state, which is with a significant CT character. This is supported by a much smaller *D* parameter (25 mT) and the vanished ZFS *E* parameter for the T_2 state ($E = 0$). This postulate is also supported by the molecular orbital analysis; for T_1 state, the overlap index of the HOMO and LUMO molecular orbitals is 0.8, whereas for T_2, the overlap index decreases to 0.58; thus T_2 state has a more significant CT character. For **Cz-AnCN**, a ^{3}LE state was observed in the TREPR spectrum, which has a ZFS *D* value of 69 mT (Fig. 9b).

The ISC of these two compounds is probably *via* the SOCT-ISC. The molecular geometry supports this postulate. The dihedral angle between the diphenyl moiety or carbazole and the cyanoanthryl moiety is 64°, and it is 81.1° in **DPA-AnCN**. The orthogonal geometry is beneficial for the conservation of the angular momentum during ISC.[31] The ESP of the triplet state, which is localized on the anthryl moiety, also supports the SOCT-ISC mechanism. For **DPA-AnCN**, the ESP phase pattern is (*a*, *e*, *a*, *e*, *a*, *e*), for **Cz-AnCN**, it is (*e*, *a*, *e*, *a*, *e*, *a*). These ESP phase patterns are neither the triplet state formed by the ordinary SOC-ISC, which should show (*e*, *e*, *e*, *a*, *a*, *a*) or (*a*, *a*, *a*, *e*, *e*, *e*), nor the triplet state formed by the RP-ISC, for which the ESP phase pattern of the triplet state is (*a*, *e*, *e*, *a*, *a*, *e*) or (*e*, *a*, *a*, *e*, *e*, *a*).[40] Previously with the julolidine–anthryl dyad, the ^{3}An state formed *via* the SOCT-ISC mechanism shows ESP of (*e*, *a*, *e*, *a*, *e*, *a*).[48] With phenothiazine–anthryl compact orthogonal dyad, we observed the ^{3}An state with ESP of (*a*, *e*, *a*, *e*, *a*, *e*).[76]

Although a simplified two states model was used to rationalize the TADF,[17,27] now it is a consensus that an intermediate triplet state, *e.g.* ^{3}LE state, should be involved in the TADF process,[34,55] because the direct ISC between the states of ^{1}CT/^{3}CT is non-efficient, a spin-vibronic ISC mechanism should be involved in ISC between the ^{1}CT and ^{3}CT states.[31,55,73]

Recently Evans shows that indirect, not direct, coupling of the ^{3}CT state to the singlet manifold facilitates ISC. Vibronic coupling plays a significant role in the ISC of ^{1}CT → ^{3}LE.[73] With a few TADF emitters, Evans *et al.* confirmed that both the ^{3}CT and ^{3}LE states were observed in the TREPR spectra. This is the result of the small energy gap between the ^{3}CT and the ^{3}LE states. With a larger energy gap between the two, and high-lying ^{3}CT state, only the ^{3}LE state was detected in the TREPR spectra.[73]

The authors propose that TADF is facilitated by SOC, based on three possible mechanisms:

(I) Direct SOC between ^{1}CT and ^{3}LE states;

(II) Vibrationally enhanced SOC between ^{1}CT and ^{3}LE states;

(III) Spin-vibronic coupling between ^{1}CT and ^{3}CT *via* intermediate ^{3}LE state.

These three ISC processes can be described by the following equation of the SOC Hamiltonian (include three non-zero terms).

$$\hat{H}_{SO} = \langle \psi_{^1CT} | \hat{H}_{SO} | \psi_{^3LE} \rangle \quad (1)$$

$$+ \sum_{\alpha} \frac{\partial \langle \psi_{^1CT} | \hat{H}_{SO} | \psi_{^3LE} \rangle}{\partial Q_\alpha} \quad (2)$$

$$+ \frac{\langle \psi_{^1CT} | \hat{H}_{SO} | \psi_{^3LE} \rangle \langle \psi_{^3LE} | \hat{H}_{vib} | \psi_{^3CT} \rangle}{E_{^1CT} - E_{^3LE}} \quad (3)$$

where Ψ is the molecular wavefunction of states coupled either by the spin–orbit ($\hat{H}_{SO}$) or vibronic ($\hat{H}_{vib}$) Hamiltonian. The first term (1) is the direct SOC for ^{1}CT → ^{3}LE ISC. The second term (2) describes the contribution of the vibrational mode for the ^{1}CT → ^{3}LE process. Vibrational modes can enhance ISC in (II) because SOC matrix elements for ^{1}CT → ^{3}LE transitions depend on the nuclear degree of freedom (Q_α). The spin-vibronic coupling contribution to the ^{1}CT ↔ ^{3}CT interconversion is described by the third term (3); the ^{3}LE state is the intermediate state. These three different ISC processes will form the ^{3}LE state or the ^{3}CT state showing specific population rates of the three sublevels, *i.e.* specific ESP phase patterns for the triplet state TREPR spectra. Furthermore, due to the rotation of the ZFS principal axes during the ^{3}LE → ^{3}CT, the occurrence of spin-vibronic ISC can be judged from the population rates of the three sublevels of the ^{3}CT state. It is based on these principles, the author concluded that with a smaller ^{3}CT/^{3}LE energy gap, the spin-vibronic ISC plays a more significant role in the formation of the ^{3}CT state. Recently, with a spiro electron donor–acceptor dyad based on close-ring rhodamine and NI moieties, we also confirmed that the ^{3}CT state is formed with a ^{3}LE precursor (*via* ^{1}CT → ^{3}LE); the direct formation of the ^{3}CT state with the ^{1}CT state as the precursor is negligible.[77] Moreover, the ^{3}LE state of all the three compounds in Fig. 10 is

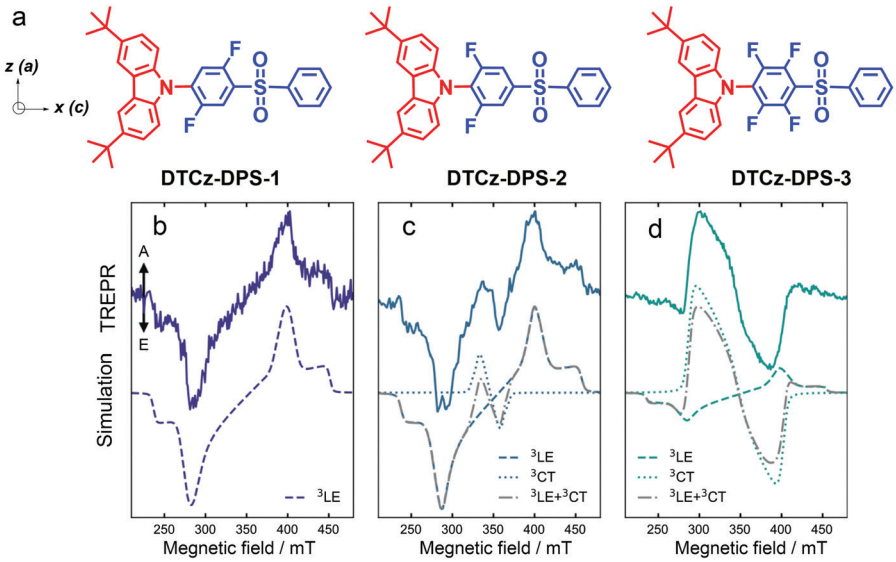

Fig. 10 (a) Molecular structures of **DTCz-DPS-1**, **DTCz-DPS-2** and **DTCz-DPS-3**. The in-plane molecular axes *a* and *c* and the ^{3}LE ZFS axes *z* and *x* are shown. Spin-polarized TREPR signals collected at 30 K in toluene for (b) **DTCz-DPS-1**, (c) **DTCz-DPS-2** and (d) **DTCz-DPS-3**. Solid lines show the TREPR signal recorded 2 μs after 355 nm laser excitation and integrated over 1 μs. Dashed and dotted lines are the simulated local excitation triplet state (^{3}LE) and charge transfer triplet state (^{3}CT) polarization patterns, respectively. Dash-dot grey lines are the weighted sums of the ^{3}LE and ^{3}CT simulations. The spin-polarized patterns are characterized by absorptive (A) and emissive (E) features. Reproduced with permission.[73] Copyright 2021, Springer Nature.

formed with the vibrational enhanced ISC, not a direct SOC effect. This information gives important insights for the future design of TADF emitters based on the electron donor–acceptor molecular structure motif.

The compounds in Fig. 10 are with variable CT state energy, because of the difference in the electron withdrawal ability of the fluorinated phenyl linker, but the ^{3}LE state energy (localized on the carbazole units) is kept consistent. From **DTCz-DPS-1** to **DTCz-DPS-3**, the electron acceptor becomes stronger, thus the CT state energy decreases in order of 3.42 eV, 3.40 eV and 3.32 eV, respectively, whereas the ^{3}LE state energy of the three compounds is kept as 3.05 eV (Table 2). Biexponential decay was observed for the luminescence of all the compounds (Table 2), but the contribution of the delayed fluorescence to the total luminescence is different for the three compounds. The energy gaps between the low-lying ^{3}LE state and the ^{3}CT state are 104 meV, 81 meV and 33 meV, respectively.

For **DTCz-DPS-1**, a triplet TREPR spectrum with the (*e*, *e*, *e*, *a*, *a*, *a*) phase pattern was observed. Simulation of the spectrum gives the ZFS *D* and *E* parameters of −108 mT and −9 mT, respectively. Thus this state can be assigned to a ^{3}LE state confined on the carbazole moiety; this is supported by the ZFS *D* of the triplet state of native carbazole 107 mT.[78] For **DTCz-DPS-2** and **DTCz-DPS-3**, however, two triplet states are required for satisfactory simulation of the experimental TREPR spectra. For **DTCz-DPS-2**, one triplet is with ZFS *D* and *E* parameters of −108 mT and −9 mT, respectively (Table 3). This state is a carbazole-localized ^{3}LE state, similar to that of **DTCz-DPS-1**. The second triplet state is with a much smaller ZFS *D* parameter of −23 mT, indicating it is a ^{3}CT state. Note the ZFS *E* parameter is not vanishing, which is determined as −3 mT. The weight of the ^{3}CT state in the total TREPR spectra is 10%. Similar TREPR results were observed for **DTCz-DPS-3**. Both ^{3}LE and ^{3}CT states were observed in the TREPR spectra, the weight of the ^{3}CT state increases to 80% in the TREPR spectra.

The authors propose that the ESP phase pattern of the ^{3}LE state indicates the ISC mechanism is not *via* HFI, *i.e.* the RP-ISC mechanism does not contribute to the formation of the ^{3}LE state. The authors stated that the ^{3}LE state is populated *via* the vibrational SOC, because the in-planes sublevels are over

Table 2 Experimental and TDDFT calculated excited-state properties. Reproduced with permission.[73] Copyright 2021, Springer Nature

Compound	λ_{PL}[a] (nm)	S_1[b] (eV)	T_1[b] (eV)	τ_{PF}[c] (ns)	τ_{DF}[c] (μs)	% delayed[d]	H_{SO}[e] (cm^{-1})	ΔG[f] (meV)
DTCz-DPS-1	438	3.42	3.05	15	11	3	0.31	104
DTCz-DPS-2	449	3.40	3.05	17	31	28	0.27	81
DTCz-DPS-3	527	3.32	3.05	5	15	37	0.32	33

[a] Photoluminescence charge-transfer transition peak maxima in deaerated toluene at 295 K. [b] The energetic onset of photoluminescence (S_1) and phosphorescence (T_1) in deaerated toluene at 77 K. [c] Prompt fluorescence lifetime (±5 ns) and delayed fluorescence lifetime (±100 ns) from integrated photoluminescence kinetics, recorded in deaerated toluene at 295 K. [d] Contribution of delayed fluorescence component to total photoluminescence from integrated time-resolved photoluminescence measured in deaerated toluene at 295 K. [e] Root sum square of the *x*, *y*, *z* components of the calculated $\langle\psi_{^1CT}|\hat{H}_{SO}|\psi_{^3LE}\rangle$ at optimized ^{3}LE geometry. [f] Difference in Gibbs free energy associated with ^{3}LE and ^{3}CT minima at their optimized geometries.

Table 3 Zero-filed splitting parameters (D and E) and spin sublevel populations ($P_{x,y,z}$) of ^{3}LE and ^{3}CT obtained by simulation of the TREPR signal detected at 30 K in deoxygenated toluene or by calculation of TDDFT optimized excited-state geometries.[a] Reproduced with permission.[73] Copyright 2021, Springer Nature

	^{3}LE parameters				^{3}CT parameters			
Compounds	Experimental D, E (mT)	Calculated D, E (mT)	$P_{x,y,z}$	Weight	Experimental D, E (mT)	Calculated D, E (mT)	$P_{x,y,z}$	Weight
DTCz-DPS-1	−108, −9	−115, −10	0.38, 0.00,0.62	1.0	—	—	—	—
DTCz-DPS-2	−110, −10	−110, −8	0.4, 0.0, 0.6	0.9	−23, −3	−76, −16	0.4, 0.6, 0.0	0.1
DTCz-DPS-3	−110, −8	−112, −9	0.4, 0.0, 0.6	0.2	−56, −19	−94, −17	0.6, 0.4, 0.0	0.8

[a] The $P_{x,y,z}$ uncertainty is ±0.1 in all cases except for **DTCz-DPS-1** ^{3}LE, which has an uncertainty of ±0.01. The weighing factor corresponds to the contribution of each ^{3}LE or ^{3}CT simulation to its total simulated spectrum.

populated. Direct SOC ISC will give different population rates of the sublevels of the ^{3}LE state, which was not observed in the experimental TREPR spectra. Based on the ESP of the ^{3}LE and the ^{3}CT states, and the mutual orientation of the donor and acceptor (there should be ZFS axes rotation for the internal conversion from ^{3}LE to ^{3}CT), the authors propose that the ^{3}CT state is populated by internal conversion from the ^{3}LE state, aided by the spin-vibronic coupling effect. Spin-vibronic induced ISC in TADF emitters with a smaller ^{3}CT/^{3}LE state energy gap is supported by the more significant ^{3}CT state weight in the TREPR spectra (Fig. 10c).

The insights into TADF photophysics attained with the TREPR spectra show that the ^{3}LE state must be close to the CT state in energy. Moreover, the ^{1}CT → ^{3}LE must be efficient. As shown by the compact electron donor–acceptor dyads, one factor enhancing the ^{1}CT → ^{3}LE is the orthogonal geometry of the π-conjugation planes of the electron donor and acceptor units in the emitter molecule. The observed ESP of the ^{3}LE state TREPR spectrum excludes the HFI induced ISC (*i.e.* RP-ISC mechanism). Moreover, vibration mode concerning the rotation of the linker between the electron donor and acceptor may increase the ISC of the TADF emitters (according to term (2)). Thus, previously proposed methods of increasing the molecular rigidity, to increase the TADF luminescence quantum yield and to maintain a narrow emission band, actually may reduce the TADF performance of the emitter.

3. Summary and prospect

In summary, the recent developments in the study of TADF emitters for application in OLEDs using time-resolved electron paramagnetic resonance (TREPR) spectroscopy were summarized, the transient species involved in the process of TADF molecular photophysics was discussed, and the influence of energy gap, vibrational and spin-vibronic coupling between the triplet charge transfer state (^{3}CT) and the localized triplet excited state (^{3}LE) on the TADF process was also analyzed. This spectroscopic method is unique in that it selectively detects the transient paramagnetic species involved in the TADF process, for instance, ^{3}CT and ^{3}LE states. Note in most cases these states are mixed with different extent CT/LE features; this character can be well probed by the TREPR spectra. Moreover, based on the electron spin polarization (ESP) phase patterns of the triplet state TREPR spectra, the orientation of the zero field splitting (ZFS) principal axes, different ISC mechanisms involved in the TADF process can be discriminated, *i.e.* the direct SOC, the vibrationally enhanced ISC, and the spin-vibronic ISC (non-Born–Oppenheimer effect). These different ISC mechanisms are difficult to be discriminated by the transient optical spectroscopic methods. Moreover, it should be pointed out that the real TADF process in the OLED device, in which the excitons are formed electronically, *i.e.* by electron–hole recombination (charge recombination), may be different from that under photoexcitation conditions.[79] The process involving different intermediate excited states was observed under different excitation conditions, *i.e.* localized triplet states are only detected upon photoexcitation, but not upon electronic excitation.[79] For the TADF molecules, photoexcitation will firstly produce the ^{1}CT state (either by direct S_0 → ^{1}CT excitation, or by ultrafast charge separation, *i.e.* ^{1}LE → ^{1}CT transition), then the triplet state ^{3}LE will be populated, subsequently the ^{3}CT state will be formed, mostly *via* ^{3}LE → ^{3}CT (note these are simplified situations). In an operating OLED device, however, the ^{1}CT and ^{3}CT (and ^{3}LE state) states will be produced directly from the excitons (*i.e.* by charge recombination), or by energy transfer from the host molecules, in which case, no ISC is required for the formation of the ^{3}CT state, although the ISC and reverse ISC (rISC) will take place after the initial states are formed. Therefore, the photophysics of the TADF molecules may not be exactly the same for photoexcitation and electronic excitation.

Moreover, one should keep in mind that TREPR spectroscopy is not a non-invasive method to probe the TADF photophysical processes, because when an external magnetic field is applied, the photophysical processes may be altered by the magnetic field, especially when the energy gap between different states is comparable to the Zeeman splitting magnitude. For the X-band EPR with an energy magnitude of *ca.* 10 μeV, normally the effect on the photophysical processes is negligible, although the RP-ISC efficiency can be affected by external magnetic fields. For the W-band or Q-band spectrometer (with the magnitude of the hundreds of μeV and meV, respectively), the energy of the magnetic field is large enough to influence the TADF photophysical processes significantly. These factors need to be considered in the future study of TADF materials using the TREPR spectra. Moreover, normally the study of the triplet states with TREPR spectra are performed in a frozen solution at cryogenic temperature, to suppress molecular tumbling and spin lattice

relaxation, but these experimental conditions can also affect the photophysical processes, for instance the CT state energy and the kinetics of the charge transfer. Concerning these aspects, TREPR spectral study of the TADF molecules in film or liquid crystal is desired, but the related reports are rare. There is still more room to unravel the general principles governing the efficient TADF process in the electron donor–acceptor based emitters for application in OLEDs.

Conflicts of interest

There are no conflicts to declare.

Acknowledgements

J. Zhao thanks the NSFC (U2001222, 21673031 and 21761142005), the Fundamental Research Funds for the Central Universities (DUT19TD28) and the State Key Laboratory of Fine Chemicals of Dalian University for financial support.

Notes and references

1 H. Yersin, *Highly Efficient OLEDs with Phosphorescent Materials*, Wiley-VCH Verlag GmbH, 2008.
2 M. Godumala, S. Choi, M. J. Cho and D. H. Choi, *J. Mater. Chem. C*, 2016, **4**, 11355–11381.
3 Y. Im, S. Y. Byun, J. H. Kim, D. R. Lee, C. S. Oh, K. S. Yook and J. Y. Lee, *Adv. Funct. Mater.*, 2017, **27**, 1603007.
4 X. Cao, D. Zhang, S. Zhang, Y. Tao and W. Huang, *J. Mater. Chem. C*, 2017, **5**, 7699–7714.
5 M. Y. Wong and E. Zysman-Colman, *Adv. Mater.*, 2017, **29**, 1605444.
6 X. Cai and S.-J. Su, *Adv. Funct. Mater.*, 2018, **28**, 1802558.
7 Y. Xu, P. Xu, D. Hu and Y. Ma, *Chem. Soc. Rev.*, 2021, **50**, 1030–1069.
8 J. Zhang, F. Zhao, X. Zhu, W.-K. Wong, D. Ma and W.-Y. Wong, *J. Mater. Chem.*, 2012, **22**, 16448–16457.
9 S. Wang, Z. Cheng, X. Song, X. Yan, K. Ye, Y. Liu, G. Yang and Y. Wang, *ACS Appl. Mater. Interfaces*, 2017, **9**, 9892–9901.
10 Z.-Y. Wang, L.-Y. Zhang, L.-J. Xu, L.-X. Shi, J.-Y. Wang and Z.-N. Chen, *ACS Appl. Mater. Interfaces*, 2021, **13**, 14433–14439.
11 H. Tian, D. Liu, J. Li, M. Ma, Y. Lan, W. Wei, R. Niu and K. Song, *New J. Chem.*, 2021, **45**, 11253–11260.
12 D. Jacquemin and D. Escudero, *Chem. Sci.*, 2017, **8**, 7844–7850.
13 W. C. Chen, C. Sukpattanacharoen, W. H. Chan, C. C. Huang, H. F. Hsu, D. Shen, W. Y. Hung, N. Kungwan, D. Escudero, C. S. Lee and Y. Chi, *Adv. Funct. Mater.*, 2020, **30**, 2002494.
14 W. Liu, L. Zhou, L. Y. Jin, W. Xie, C.-M. Che and G. Cheng, *J. Mater. Chem. C*, 2021, **9**, 3384–3390.
15 N. J. Turro, V. Ramamurthy and J. C. Scaiano, *Principles of Molecular Photochemistry: An Introduction*, University Science Books, Sausalito, CA, 2009.
16 A. Endo, M. Ogasawara, A. Takahashi, D. Yokoyama, Y. Kato and C. Adachi, *Adv. Mater.*, 2009, **21**, 4802–4806.
17 H. Uoyama, K. Goushi, K. Shizu, H. Nomura and C. Adachi, *Nature*, 2012, **492**, 234–238.
18 Y. Tao, K. Yuan, T. Chen, P. Xu, H. Li, R. Chen, C. Zheng, L. Zhang and W. Huang, *Adv. Mater.*, 2014, **26**, 7931–7958.
19 Q. Peng, D. Fan, R. Duan, Y. Yi, Y. Niu, D. Wang and Z. Shuai, *J. Phys. Chem. C*, 2017, **121**, 13448–13456.
20 M. Li, Y. Liu, R. Duan, X. Wei, Y. Yi, Y. Wang and C.-F. Chen, *Angew. Chem., Int. Ed.*, 2017, **56**, 8818–8822.
21 T. T. Bui, F. Goubard, M. Ibrahim-Ouali, D. Gigmes and F. Dumur, *Beilstein J. Org. Chem.*, 2018, **14**, 282–308.
22 X. Zhang, D. Jacquemin, Q. Peng, Z. Shuai and D. Escudero, *J. Phys. Chem. C*, 2018, **122**, 6340–6347.
23 Z. Cheng, Z. Li, Y. Xu, J. Liang, C. Lin, J. Wei and Y. Wang, *ACS Appl. Mater. Interfaces*, 2019, **11**, 28096–28105.
24 L. Wang, Q. Ou, Q. Peng and Z. Shuai, *J. Phys. Chem. A*, 2021, **125**, 1468–1475.
25 Y. Mei, D. Liu, J. Li, H. Li and W. Wei, *J. Mater. Chem. C*, 2021, **9**, 5885–5892.
26 H. Tanaka, K. Shizu, H. Miyazaki and C. Adachi, *Chem. Commun.*, 2012, **48**, 11392–11394.
27 H. Tanaka, K. Shizu, H. Nakanotani and C. Adachi, *J. Phys. Chem. C*, 2014, **118**, 15985–15994.
28 Q. Zhang, H. Kuwabara, W. J. Potscavage, S. Huang, Y. Hatae, T. Shibata and C. Adachi, *J. Am. Chem. Soc.*, 2014, **136**, 18070–18081.
29 T. J. Penfold, *J. Phys. Chem. C*, 2015, **119**, 13535–13544.
30 J. Gibson, A. P. Monkman and T. J. Penfold, *ChemPhysChem*, 2016, **17**, 2956–2961.
31 P. K. Samanta, D. Kim, V. Coropceanu and J.-L. Brédas, *J. Am. Chem. Soc.*, 2017, **139**, 4042–4051.
32 Z.-W. Li, L.-Y. Peng, X.-F. Song, W.-K. Chen, Y.-J. Gao, W.-H. Fang and G. Cui, *J. Phys. Chem. Lett.*, 2021, **12**, 5944–5950.
33 M. K. Etherington, J. Gibson, H. F. Higginbotham, T. J. Penfold and A. P. Monkman, *Nat. Commun.*, 2016, **7**, 13680.
34 H. Noda, X.-K. Chen, H. Nakanotani, T. Hosokai, M. Miyajima, N. Notsuka, Y. Kashima, J.-L. Brédas and C. Adachi, *Nat. Mater.*, 2019, **18**, 1084–1090.
35 J. W. Verhoeven, H. J. van Ramesdonk, M. M. Groeneveld, A. C. Benniston and A. Harriman, *ChemPhysChem*, 2005, **6**, 2251–2260.
36 J. W. Verhoeven, *J. Photochem. Photobiol. C*, 2006, **7**, 40–60.
37 Y. Hou, X. Zhang, K. Chen, D. Liu, Z. Wang, Q. Liu, J. Zhao and A. Barbon, *J. Mater. Chem. C*, 2019, **7**, 12048–12074.
38 H. Levanon and J. R. Norris, *Chem. Rev.*, 1978, **78**, 185–198.
39 C. Hintze, U. E. Steiner and M. Drescher, *ChemPhysChem*, 2017, **18**, 6–16.
40 S. Richert, C. E. Tait and C. R. Timmel, *J. Magn. Reson.*, 2017, **280**, 103–116.
41 S. Weber, *eMagRes*, 2017, **6**, 255–270.
42 T. Biskup, *Front. Chem.*, 2019, **7**, 10.
43 M. Imran, X. Zhang, Z. Wang, X. Chen, J. Zhao, A. Barbon and V. K. Voronkova, *Phys. Chem. Chem. Phys.*, 2021, **23**, 15835–15868.

44 Z. Wang, X. Zhang and J. Zhao, *J. Phys. Chem. C*, 2021, **125**, 19097–19109.
45 S. Richert, G. Bullard, J. Rawson, P. J. Angiolillo, M. J. Therien and C. R. Timmel, *J. Am. Chem. Soc.*, 2017, **139**, 5301–5304.
46 C. Hintze, P. Korf, F. Degen, F. Schütze, S. Mecking, U. E. Steiner and M. Drescher, *J. Phys. Chem. Lett.*, 2017, **8**, 690–695.
47 Z. E. X. Dance, Q. Mi, D. W. McCamant, M. J. Ahrens, M. A. Ratner and M. R. Wasielewski, *J. Phys. Chem. B*, 2006, **110**, 25163–25173.
48 Z. E. X. Dance, S. M. Mickley, T. M. Wilson, A. B. Ricks, A. M. Scott, M. A. Ratner and M. R. Wasielewski, *J. Phys. Chem. A*, 2008, **112**, 4194–4201.
49 N. J. Turro, M. H. Kleinman and E. Karatekin, *Angew. Chem., Int. Ed.*, 2000, **39**, 4436–4461.
50 A. Kawai and K. Shibuya, *J. Photochem. Photobiol. C*, 2006, **7**, 89–103.
51 T. Ogiwara, Y. Wakikawa and T. Ikoma, *J. Phys. Chem. A*, 2015, **119**, 3415–3418.
52 M. Montalti, A. Credi, L. Prodi and M. T. Gandolfi, *Handbook of Photochemistry*, CRC Press, Boca Raton, 2006.
53 T. Hosokai, H. Matsuzaki, H. Nakanotani, K. Tokumaru, T. Tsutsui, A. Furube, K. Nasu, H. Nomura, M. Yahiro and C. Adachi, *Sci. Adv.*, 2017, **3**, 1603282.
54 R. Ishimatsu, T. Edura, C. Adachi, K. Nakano and T. Imato, *Chem. – Eur. J.*, 2016, **22**, 4889–4898.
55 F. B. Dias, J. Santos, D. R. Graves, P. Data, R. S. Nobuyasu, M. A. Fox, A. S. Batsanov, T. Palmeira, M. N. Berberan-Santos, M. R. Bryce and A. P. Monkman, *Adv. Sci.*, 2016, **3**, 1600080.
56 D. J. Gibbons, A. Farawar, P. Mazzella, S. Leroy-Lhez and R. M. Williams, *Photochem. Photobiol. Sci.*, 2020, **19**, 136–158.
57 M. A. Filatov, *Org. Biomol. Chem.*, 2020, **18**, 10–27.
58 E. Bassan, A. Gualandi, P. G. Cozzi and P. Ceroni, *Chem. Sci.*, 2021, **12**, 6607–6628.
59 X. Zhang, Z. Wang, Y. Hou, Y. Yan, J. Zhao and B. Dick, *J. Mater. Chem. C*, 2021, **9**, 11944–11973.
60 I. Bhattacharjee, N. Acharya, H. Bhatia and D. Ray, *J. Phys. Chem. Lett.*, 2018, **9**, 2733–2738.
61 J. S. Ward, R. S. Nobuyasu, A. S. Batsanov, P. Data, A. P. Monkman, F. B. Dias and M. R. Bryce, *Chem. Commun.*, 2016, **52**, 2612–2615.
62 X. Xiong, F. Song, J. Wang, Y. Zhang, Y. Xue, L. Sun, N. Jiang, P. Gao, L. Tian and X. Peng, *J. Am. Chem. Soc.*, 2014, **136**, 9590–9597.
63 E. W. Evans, Y. Olivier, Y. Puttisong, W. K. Myers, T. J. H. Hele, S. M. Menke, T. H. Thomas, D. Credgington, D. Beljonne, R. H. Friend and N. C. Greenham, *J. Phys. Chem. Lett.*, 2018, **9**, 4053–4058.
64 B. Wex and B. R. Kaafarani, *J. Mater. Chem. C*, 2017, **5**, 8622–8653.
65 S. Kuila, A. Ghorai, P. K. Samanta, R. B. K. Siram, S. K. Pati, K. S. Narayan and S. J. George, *Chem. – Eur. J.*, 2019, **25**, 16007–16011.
66 M. Hussain, A. M. El-Zohry, Y. Hou, A. Toffoletti, J. Zhao, A. Barbon and O. F. Mohammed, *J. Phys. Chem. B*, 2021, **125**, 10813–10831.
67 G. Tang, A. A. Sukhanov, J. Zhao, W. Yang, Z. Wang, Q. Liu, V. K. Voronkova, M. Di Donato, D. Escudero and D. Jacquemin, *J. Phys. Chem. C*, 2019, **123**, 30171–30186.
68 A. Demeter, L. Biczok, T. Berces, V. Wintgens, P. Valat and J. Kossanyi, *J. Phys. Chem.*, 1993, **97**, 3217–3224.
69 X. Zhang, Y. Hou, X. Xiao, X. Chen, M. Hu, X. Geng, Z. Wang and J. Zhao, *Coordin. Chem. Rev.*, 2020, **417**, 213371.
70 S. Suzuki, R. Sugimura, M. Kozaki, K. Keyaki, K. Nozaki, N. Ikeda, K. Akiyama and K. Okada, *J. Am. Chem. Soc.*, 2009, **131**, 10374–10375.
71 Y. Kobori, M. Fuki and H. Murai, *J. Phys. Chem. B*, 2010, **114**, 14621–14630.
72 A. Karimata, H. Kawauchi, S. Suzuki, M. Kozaki, N. Ikeda, K. Keyaki, K. Nozaki, K. Akiyama and K. Okada, *Chem. Lett.*, 2013, 794–796.
73 B. H. Drummond, N. Aizawa, Y. Zhang, W. K. Myers, Y. Xiong, M. W. Cooper, S. Barlow, Q. Gu, L. R. Weiss, A. J. Gillett, D. Credgington, Y.-J. Pu, S. R. Marder and E. W. Evans, *Nat. Commun.*, 2021, **12**, 4532.
74 J. Karpiuk, A. Majka, E. Karolak and J. Nowacki, *J. Phys. Chem. Lett.*, 2017, **8**, 4659–4667.
75 N. Sharma, M. Y. Wong, D. Hall, E. Spuling, F. Tenopala-Carmona, A. Privitera, G. Copley, D. B. Cordes, A. M. Z. Slawin, C. Murawski, M. C. Gather, D. Beljonne, Y. Olivier, I. D. W. Samuel and E. Zysman-Colman, *J. Mater. Chem. C*, 2020, **8**, 3773–3783.
76 Y. Hou, T. Biskup, S. Rein, Z. Wang, L. Bussotti, N. Russo, P. Foggi, J. Zhao, M. Di Donato, G. Mazzone and S. Weber, *J. Phys. Chem. C*, 2018, **122**, 27850–27865.
77 D. Liu, A. M. El-Zohry, M. Taddei, C. Matt, L. Bussotti, Z. Wang, J. Zhao, O. F. Mohammed, M. Di Donato and S. Weber, *Angew. Chem., Int. Ed.*, 2020, **59**, 11591–11599.
78 I. S. M. Saiful, P. Heinze, Y. Ohba, S. Yamauchi, M. Yamamoto, Y. Tohda and K. Tani, *Mol. Phys.*, 2006, **104**, 1535–1542.
79 N. Bunzmann, S. Weissenseel, L. Kudriashova, J. Gruene, B. Krugmann, J. V. Grazulevicius, A. Sperlich and V. Dyakonov, *Mater. Horiz.*, 2020, **7**, 1126–1137.